

Article

Preparation of CaO@CeO₂ Solid Base Catalysts Used for Biodiesel Production

Wilasinee Kingkam ^{1,*}, Jirapa Maisomboon ¹, Khemmanich Khamenkit ¹, Sasikarn Nuchdang ¹, Kewalee Nilgumhang ², Sudarat Issarapanacheewin ³ and Dussadee Rattanaphra ^{1,*}

¹ Nuclear Technology Research and Development Center, Thailand Institute of Nuclear Technology (Public Organization), Ongkharak, Nakhon Nayok 26120, Thailand; ming-mafia@hotmail.com (J.M.); khemmanich.kk@gmail.com (K.K.); sasikarn@tint.or.th (S.N.)

² Nuclear Fusion and Plasma Section (NFPS), Thailand Institute of Nuclear Technology (Public Organization), Ongkharak, Nakhon Nayok 26120, Thailand; kewalee@tint.or.th

³ Radioactive Waste Management Center, Thailand Institute of Nuclear Technology (Public Organization), Ongkharak, Nakhon Nayok 26120, Thailand; sudarat@tint.or.th

* Correspondence: wilasinee@tint.or.th (W.K.); dussadeer@tint.or.th (D.R.)

Abstract: The study investigated the use of CeO₂ extracted from monazite with calcium oxide (CaO) as a solid catalyst for biodiesel production. The wet impregnation method was used to produce CaO@CeO₂ mixed-oxide catalysts with 0–50 wt.% CaO. X-ray diffraction (XRD), Brunauer–Emmett–Teller (BET) surface area analysis, thermogravimetric analysis (TGA), and a Fourier transform infrared spectrometer (FTIR) was used to characterize the catalysts. In order to determine the optimal preparation conditions, the effect of different CaO compositions on the performance of CaO@CeO₂ mixed-oxide catalysts was examined. The catalytic activity of the CaO@CeO₂ catalyst for the transesterification reaction of palm oil to produce biodiesel was studied. The results show that the optimum yield of biodiesel can reach 97% fatty acid methyl ester over the 30CaO@CeO₂ catalyst at the reaction conditions of 5 wt.% catalysts, methanol-to-oil molar ratio of 9:1, with a reaction temperature of 65 °C within 30 min. The results show that the high catalytic activity and stability of the CaO@CeO₂ catalyst make it a promising candidate for industrial-scale biodiesel production. Further study is needed to improve the stability and efficiency of catalysts in transesterification reactions to achieve a high FAME yield using long-life-span catalysts. Moreover, it is necessary to investigate the economic feasibility of this process for application in large-scale biodiesel production.

Keywords: biodiesel; transesterification; cerium oxide; impregnation; palm oil



Citation: Kingkam, W.; Maisomboon, J.; Khamenkit, K.; Nuchdang, S.; Nilgumhang, K.; Issarapanacheewin, S.; Rattanaphra, D. Preparation of CaO@CeO₂ Solid Base Catalysts Used for Biodiesel Production. *Catalysts* **2024**, *14*, 240. <https://doi.org/10.3390/catal14040240>

Academic Editor: Claudia Carlucci

Received: 21 February 2024

Revised: 18 March 2024

Accepted: 20 March 2024

Published: 4 April 2024



Copyright: © 2024 by the authors. Licensee MDPI, Basel, Switzerland. This article is an open access article distributed under the terms and conditions of the Creative Commons Attribution (CC BY) license (<https://creativecommons.org/licenses/by/4.0/>).

1. Introduction

People have widely begun to focus on low-carbon, ecologically friendly, clean, and safe renewable resources due to the scarcity of fossil fuels, environmental contamination, and ecological deterioration [1,2], due to their renewable, biodegradable, non-toxic nature, and safety for both people and the environment. Thailand is currently dependent on imported energy sources for over half of its energy requirements; this reliance on foreign sources is expected to intensify as oil and gas reserves diminish. Fuel consumption rose by 2.3% year-on-year in the first nine months of 2023 to 154 million liters per day on average, in line with the country's economic growth, which tends to increase oil consumption every year. Furthermore, the growing human energy demand has led to a crisis in the diesel price, which has been rising continuously. The government has recognized the criticality of increasing domestic renewable energy production to decrease reliance on crude imports. Thus, biodiesel has gained more and more attention in recent years. Several techniques can be used for the production of biodiesel. The direct blending technique and the microemulsion method cannot produce diesel fuel standards [3], whereas biodiesel produced by the esterification and transesterification methods has properties very similar

to petrochemical fuels and it can be used in diesel engines without the modification of biodiesel. Homogeneous catalytic transesterification, which uses H_2SO_4 , NaOH , or KOH , is now the primary industry production technique for biodiesel generation [4]. However, there are significant drawbacks to homogeneous catalytic transesterification. Thus, heterogeneous catalysts in transesterification reactions provide advantages over homogeneous transesterification reactions by being easily separated, reusable, and free from saponification reactions [5]. Additionally, heterogeneous catalysts often exhibit higher catalytic activity and selectivity compared to homogeneous catalysts. This can lead to improved efficiency and yield in transesterification processes.

Many researchers have reported that alkaline earth metal oxides have the ability to produce a higher biodiesel yield due to their superior physicochemical properties and that the high pore diameter, pore volume, crystallite size, and surface area [6] at the edges of the metal oxide are among the most important factors influencing the catalytic performance in transesterification reactions. In the alkaline earth metal group, CaO is a potential alkaline earth metal catalyst that has shown high catalytic activity and is environmentally friendly [7]. However, during transesterification reactions, the leached Ca species will react with free fatty acids (FFAs) and easily form soap [8,9]. As a result, supporting CaO onto carriers such as transition metal oxides or Ca -containing perovskites can further increase the stability of bulk CaO . Cerium oxide (CeO_2) is highly significant as a catalytic material because of its distinctive acid–base and redox characteristics [10]. Utilizing CeO_2 mixed oxides is an advantageous approach to alter the physical and chemical characteristics of oxides. This process results in a reduction in crystal domain size, an increase in surface area, and the presence of many oxygen vacancies. Compared to other CaO -based catalysts that have been studied so far, the CaO - CeO_2 catalyst has shown great promise in transesterification reactions. Wong et al. [11] have synthesized solid base CaO - CeO_2 mixed-oxide catalysts via wet impregnation. An optimal biodiesel yield of 95% was obtained using the 50Ca-Ce catalyst, which may be reused up to six times without a loss of catalytic activity. Kawashima et al. [12] studied the transesterification of rapeseed oil using a CaO - CeO_2 catalyst. A 90% biodiesel production was achieved at the optimal conditions of 60 °C with a 6:1 molar ratio of methanol to oil at a reaction time of 10 h. The utilization of CaO - CeO_2 supporting metallic monolithic catalysts for biodiesel production achieved a sunflower oil conversion rate of around 99%. However, significant leaching of the active catalytic layer occurred in the second reaction cycle, as reported by Reyero et al. [13]. In the transesterification process, CeO_2 is found to be inactive. The interaction between calcium oxide and cerium oxide, on the other hand, may reduce CaO leaching in biodiesel products when calcium oxide is mixed with cerium oxide [14,15].

In this study, CaO@CeO_2 mixed-oxide catalysts have been developed to improve the physicochemical properties and catalytic activity of CaO@CeO_2 towards palm oil in the transesterification reaction. The effects of various CaO loadings on BET surface area with respect to biodiesel FAME yield were studied. In addition to investigating the stability and catalytic activity of the catalyst in transesterification reactions, its reusability in repeated bulk reactions was estimated.

2. Results

2.1. Catalysts Characterization

X-ray diffraction (XRD) patterns for the CaO@CeO_2 catalysts with different Ce contents are given in Figure 1. The diffraction peaks for each sample were distinct and displayed patterns that were consistent. The peaks at 28.55°, 33.07°, 47.48°, 56.34°, and 59.09° from (111), (200), (220), (311), and (222) were indicative of pure CeO_2 with a cubic structure (JCPDS No: 43-1002). The cubic structure of pure CaO showed clearly defined diffraction peaks at 2θ values of 32.20°, 37.36°, 53.86°, 64.15°, and 67.37° corresponding to a cubic crystal structure (JCPDS No: 43-1001) associated with reflections from the (111), (200), (220), (311), and (222) planes, respectively. A part of the XRD pattern of these $x\text{CeO}_2@\text{CaO}$ catalysts revealed that these samples had distinct crystalline phases of CaO , $\text{Ca}(\text{OH})_2$,

and CeO_2 [16]. In these samples, no new chemical was identified. In addition to the reflections from the $\text{CeO}_2@/\text{CaO}$ phase, three minor and less intense peaks were observed at 2θ values of 28.6° , 34.1° , and 50.7° , which can be assigned to the $\text{Ca}(\text{OH})_2$ phase with a hexagonal structure (JCPDS No: 78-0315). The average crystalline size of the $\text{CaO}@\text{CeO}_2$ was calculated using XRD analysis data, and the Debye–Scherrer equation for CeO_2 , CaO , $30\text{CaO}@\text{CeO}_2$, $40\text{CaO}@\text{CeO}_2$, and $50\text{CaO}@\text{CeO}_2$ yielded 15.24, 39.10, 24.64, 17.85, and 18.87 nm, respectively.

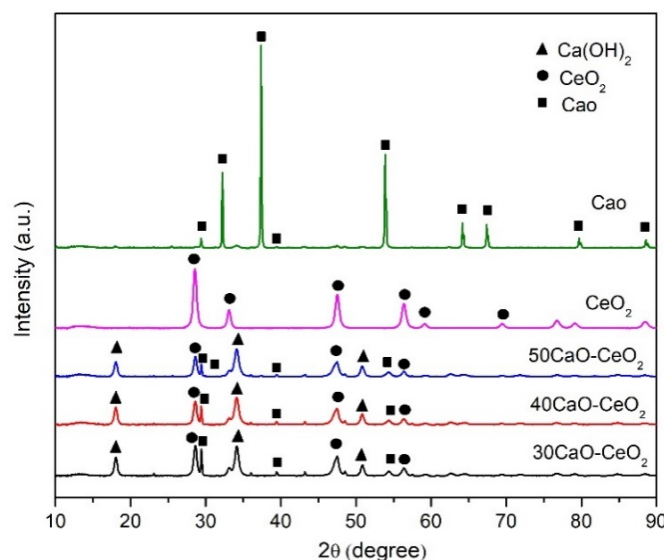


Figure 1. XRD patterns of the $x\text{CaO}@\text{CeO}_2$ catalysts.

The presence of CaO was verified by the XRF, XRD, and FTIR analyses. The XRF analysis of the catalysts revealed the weight percentage of different compounds, including CeO_2 (Table 1). Moreover, CaO was the most abundant as compared to the other compounds, followed by CeO_2 , P_2O_5 , SO_3 , and SiO_2 , respectively. With the increase in CaO content, the CeO_2 content decreased in concentration from 17.92 to 12.28%. The crystallite sizes of catalysts decreased with the increase in CaO . As previous research reported [17], CeO_2 is most commonly used as a catalyst or as a non-inert support for catalysts due to its abundant oxygen vacancies, strong interaction with metals, and controllable synthesis with different exposed crystal facets. Thus, the increase in CeO_2 content greatly improved the catalytic activity and stability of the $30\text{CaO}@\text{CeO}_2$ catalysts in transesterification reactions for biodiesel production. In Table 2, the $\text{CaO}@\text{CeO}_2$ catalysts' surface areas, pore volumes, pore diameters, and crystallite sizes are listed. The surface areas and pore volumes of the samples increased from $34.49 \text{ m}^2/\text{g}$ to $53.30 \text{ m}^2/\text{g}$ and from $0.11 \text{ cm}^3/\text{g}$ to $0.16 \text{ cm}^3/\text{g}$, respectively, when the CaO content in the catalysts increased from 30 to 50 wt.%.

The data obtained from the nitrogen adsorption–desorption of the CaO , CeO_2 , and $x\text{CaO}@\text{CeO}_2$ catalysts are presented in Table 2. In general, pore volume, high surface area, and porosity improvement all affect the absorption capacity. The surface area of CeO_2 with 50 wt.% CaO was higher than that of pure CeO_2 . As the CaO content support in CeO_2 catalysts increased from 0 wt.% to 50 wt.%, the surface areas and pore volumes of the samples increased significantly from 34.49 to 53.30 and $0.09 \text{ cm}^3/\text{g}$ to $0.16 \text{ cm}^3/\text{g}$, respectively. An increase in BET surface area is known to enhance catalytic activity. In this case, the FAME yield decreased with increasing Ca , possibly due to alterations in the active sites on the catalyst surface caused by the addition of Ca as reported by Yu et al. [18]. While the pore diameters of all the samples were in the range of 8–10 nm, they were classified as mesoporous because the pore diameters ranged from 2 nm to 50 nm [19,20]. This is advantageous for large-reactant reactions because mesopore catalysts may decrease the transesterification reaction's pore diffusion limits in biodiesel production [21–23]. This is because larger pores promote reactant diffusion into pore channels, which increases

their access to a large number of active sites [24]. The average crystallite size of the CaO, CeO₂, and xCaO@CeO₂ catalysts was calculated as 15.24–39.10 nm using Debye–Scherrer’s equation. The study also demonstrated that the size of the crystallites and particle size in the CaO@CeO₂ catalysts decreased as the concentration of CaO increased. This result corresponded with the XRD results, showing that higher levels of CaO loading resulted in smaller crystallite and particle sizes, leading to a high surface area [25,26]. This indicates that a larger crystallite size could potentially improve the catalytic activity in biodiesel production, as reported by Thunyaratchatanon et al. [27]. Moreover, the large pore size was related to the large number of active sites within the catalyst pores. This facilitated the enhanced access of the reactants to the catalyst’s active site [28,29], which exhibited high catalytic activity in the transesterification reaction of palm oil with 97.6% FAME.

Table 1. XRF Analysis of CaO, CeO₂, and xCaO@CeO₂ catalysts.

Formular	Concentration (%)				
	CaO	CeO ₂	30CaO@CeO ₂	40CaO@CeO ₂	50CaO@CeO ₂
CaO	97.48	0.30	79.92	84.14	85.28
CeO ₂	-	99.02	17.92	13.33	12.28
MgO	0.93	-	0.66	0.71	0.76
P ₂ O ₅	0.38	-	0.53	0.51	0.43
SO ₃	0.37	-	0.39	0.39	0.41
SiO ₂	0.35	0.19	0.37	0.38	0.40
Al ₂ O ₃	0.20	0.06	-	0.29	0.20
Fe ₂ O ₃	0.19	0.03	0.17	0.18	0.18
K ₂ O	0.05	-	0.02	0.04	0.03
SrO	0.04	-	0.02	0.03	0.03
ZnO	-	0.06%	-	-	-
PbO	-	0.03%	-	-	-

Table 2. Surface area, pore volume, average pore diameter, and crystallite size of the CaO, CeO₂, and xCaO@CeO₂ catalysts.

Samples	Surface Area (m ² ·g ⁻¹)	Pore Volume (cm ³ ·g ⁻¹)	Pore Width (nm)	Crystallite Size (nm)	Average Particle Size (nm)
CaO	37.40	0.09	8.90	39.10	160.40
30CaO@CeO ₂	34.49	0.11	10.06	24.64	173.93
40CaO@CeO ₂	46.91	0.15	9.77	19.85	127.87
50CaO@CeO ₂	53.30	0.16	9.17	18.87	112.56
CeO ₂	39.68	0.09	8.46	15.24	151.20

The nitrogen adsorption–desorption isotherm profiles of the catalysts are shown in Figure 2. All the adsorption–desorption isotherms were of Type IV. The hysteresis loops of the CaO, 30CaO@CeO₂, 40CaO@CeO₂, and 50CaO@CeO₂ samples were of Type H3, while the CeO₂ exhibited Type H2 hysteresis loops in the IUPAC classification, indicating mesoporous materials. Figure 3 shows the pore size distribution of these catalysts calculated using the BJH method. The mesoporous ceria products, 30CaO@CeO₂, 40CaO@CeO₂, and 50CaO@CeO₂ exhibited a narrow and uniform pore size distribution in the average range of 9–10 nm. The CeO₂ material had small pores (8.46 nm) and a uniform pore size distribution.

The FTIR spectrum of the CaO, CeO₂, and modified CaO@CeO₂ catalysts is presented in Figure 4. From the results, the fundamental stretching vibration bands (Ce–O) of the CeO₂ appeared at 745 cm⁻¹ and 540 cm⁻¹, indicating the corresponding bands attributed to the metal–oxygen bond [30]. The FTIR spectrum of the modified CaO@CeO₂ catalysts showed that at low CaO loadings, strong absorption bands at 875 and a broad peak at 1420–1460 cm⁻¹ appeared, which was attributed to the presence of C–O bonds in the carbonation of calcium oxide [31,32]. These carbonate bands increased with increasing

weight percentage of CaO over the CeO₂ support. The weak peak at 3640 cm⁻¹ was attributed to the absorption of water on the modified catalyst surface and corresponded to the hydroxyl group stretching peak of hydroxide species [33–35]. These peaks corresponded to the stretching vibrations of the Ca–O bond, which indicated the presence of CaO in the prepared catalyst. The strong band at 530 cm⁻¹ identified the vibration of the Ca–O bond, showing the presence of alkyl halides adsorbed on the surface of CaO [32].

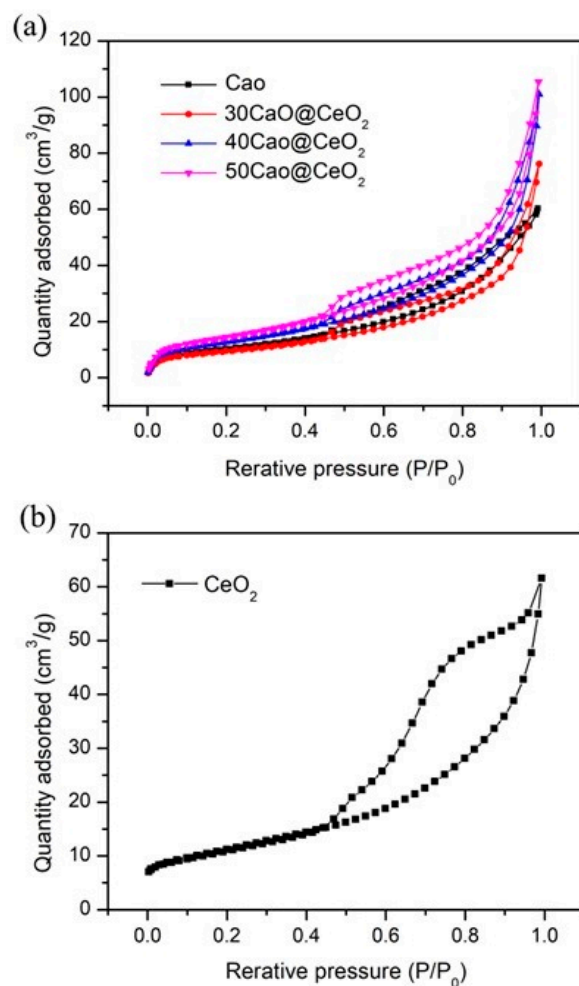


Figure 2. N₂ adsorption–desorption isotherms of (a) xCaO@CeO₂ catalysts and (b) CeO₂.

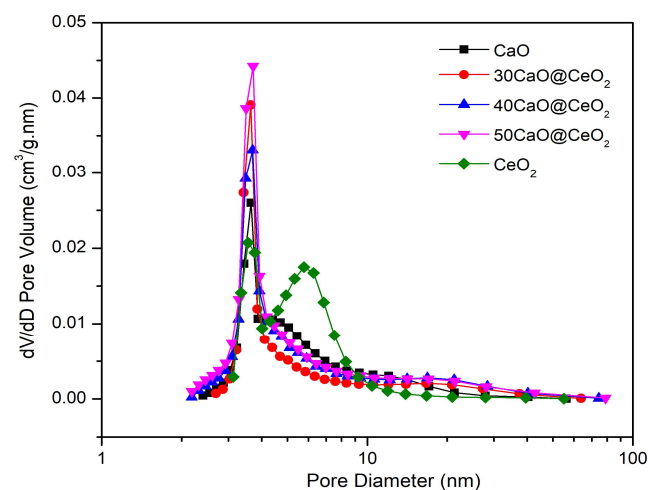


Figure 3. Barrett–Joyner–Halenda (BJH) desorption pore size distribution.

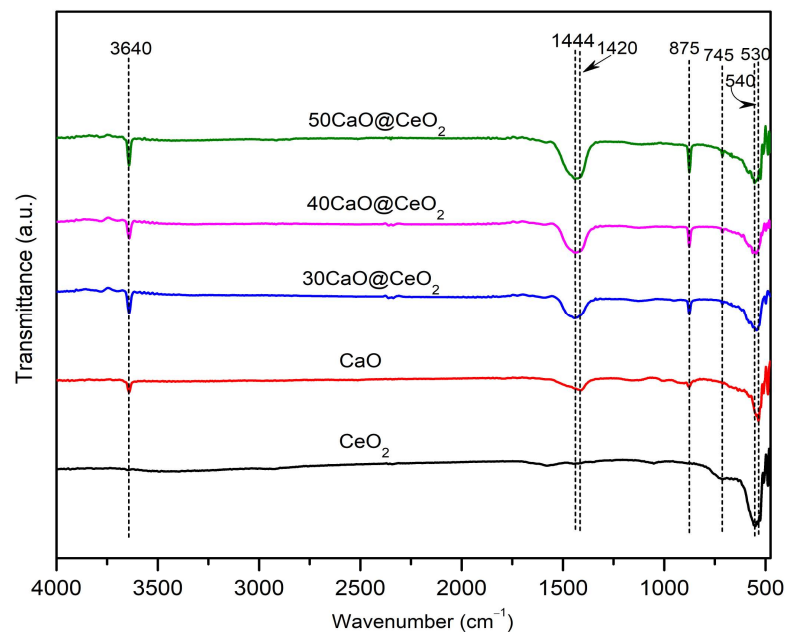


Figure 4. FTIR spectrum of CaO, CeO₂, and xCaO@CeO₂ catalysts.

TGA analysis was used to investigate the thermal stability of the CaO, CeO₂, and xCaO@CeO₂ catalysts, showing a gradual and complex degradation process (Figure 5). Except for the CeO₂ catalyst, they showed good thermal stability up to a temperature of 800 °C without any significant weight loss. The minimum loss of weight of approximately 3% was probably caused by the water absorbed on the CeO₂ surface [36]. The weight loss measurements before and after the CaO catalyst indicated that the catalyst was consumed in two stages: the combustion of complex organic compounds containing Ca and the decomposition of carbonaceous substances from glycerol on the CaO catalyst's surface [37]. It is well known that CaO is a highly reactive substance that tends to undergo carbonation and hydration within a few hours in the normal state [38]. Thus, the first state weight loss of pure CaO that happened at 400 °C was about 8%, corresponding to an endothermic peak. It was attributed to the chemically bound water decomposition of (Ca(OH)₂). In the second state, the 15% mass reduction might have been due to the loss of surface water and matrix water (Ca(OH)₂). At the same time, CO₂ reacted with the particles to form CaCO₃. Finally, the last weight loss occurred when CaCO₃ converted to the CaO form over the temperature range of 600 °C to 720 °C, where the final mass percentage was 58.71%. For the xCaO@CeO₂ catalysts, the total mass loss from 25 °C to 800 °C was found to be 60.60%, 29.64%, and 28.43% for 30CaO@CeO₂, 40CaO@CeO₂, and 50CaO@CeO₂, respectively. All curves indicated that decomposition mainly occurred in the second stage and was complete at about 800 °C. The weight loss found from the TGA measurements agreed fairly well with that expected for the decomposition of hydroxy carbonates (M₂CO₃(OH)₂) to different oxides of Ca and Ce [39,40].

The SEM images of the xCaO@CeO₂ mixed-oxide catalysts calcined at a temperature of 600 °C are depicted in Figure 6. All of the catalysts existed as irregularly formed crystalline particles. An increase in the concentration of CaO led to a steady drop in particle size, resulting in a narrow particle size distribution. These results corresponded with the surface area data analysis obtained for the CaO, CeO₂, and xCaO@CeO₂ catalysts. The surface area and pore volume of the CaO@CeO₂ catalysts increased once the crystallite size decreased, and reached its maximum value at 50CaO@CeO₂ (see Table 2).

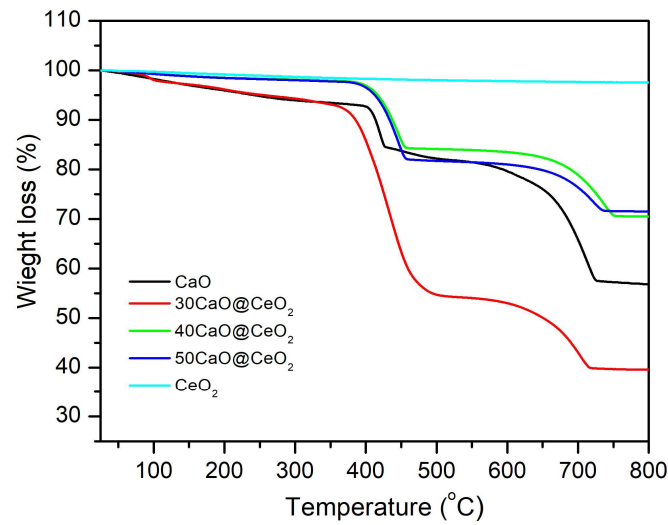


Figure 5. TGA results of the CaO, CeO₂, and xCaO@CeO₂ catalysts.

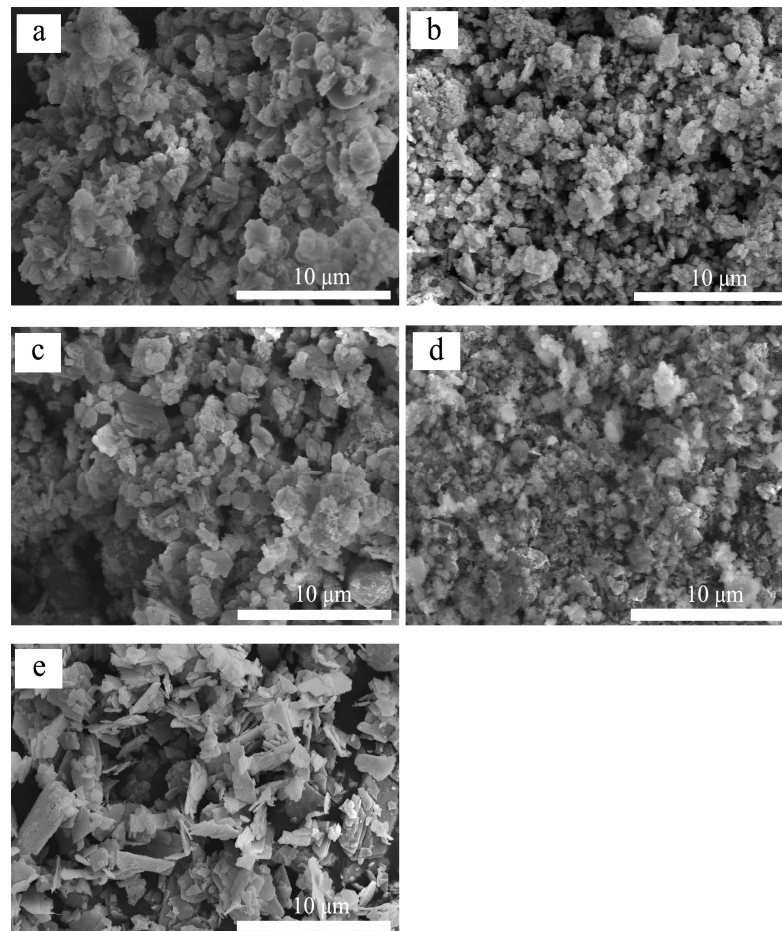


Figure 6. SEM images of (a) CaO, (b) 30CaO@CeO₂, (c) 40CaO@CeO₂, (d) 50CaO@CeO₂, and (e) CeO₂.

Figure 7 shows the EDX mapping of the 30CaO@CeO₂ catalyst. It demonstrated that only Ce, Ca, and O elements existed in the samples, and it was found that the uniform distribution of CaO covered the surface of CeO₂ completely. The EDX spectrum of the 30CaO@CeO₂ catalyst confirmed the presence of Ce, Ca, and O elements with weights of 7.6%, 33.4%, and 40.7%, respectively. This means the experimental compositions

were in good agreement with each other, with no significant deviation observed. The experimental compositions showed good agreement with the XRF results, showing no substantial variance.

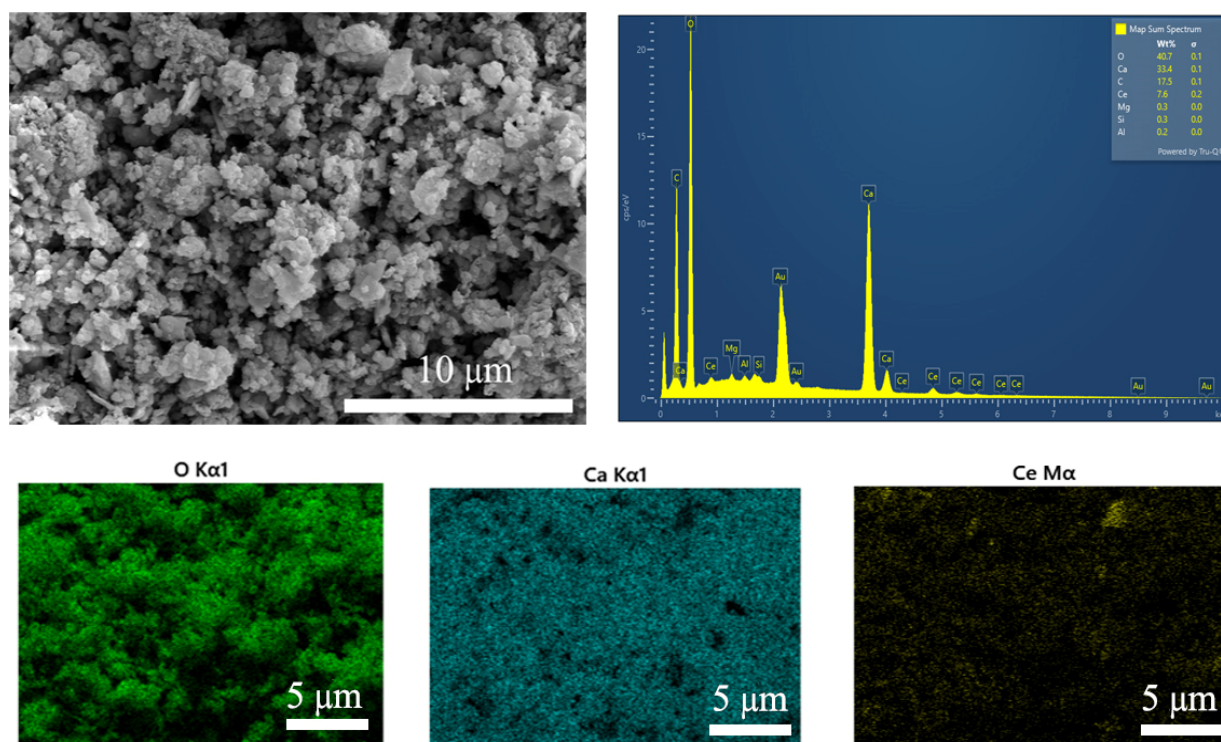


Figure 7. SEM images, EDX, and elemental mapping of the 30CaO@CeO₂ catalyst.

2.2. Catalytic Activity

The catalytic activity of different compositions of xCaO@CeO₂ catalysts, CeO₂, and CaO were studied in the transesterification of palm oil using 5 wt.% catalyst, a 9:1 methanol to oil molar ratio, a reaction temperature of 65 °C, and a reaction time of 4 h. The relationship between BET surface area and biodiesel yield is illustrated in Figure 8a, while Figure 8b shows the relationship between crystallite size and biodiesel yield. As calcium oxide loading in CaO@CeO₂ catalysts increased from 30 to 50 wt.%, the biodiesel yield decreased slightly (from 97.6% to 86.67%) with the crystallite size (from 24.64 to 18.87 nm), while the BET surface area increased (from 34.49 to 53.30 m²/g).

According to the results, a larger crystallite size and a high BET surface area led to a high FAME yield. Because the crystallite size in nanoparticles is related to the number of active catalyst sites and the surface area of the catalyst [41], it is one of the most significant factors for the catalyst. Moreover, the larger crystal size and the smaller surface area of the catalyst [42] demonstrated high performance in transesterification, according to the FAME yield results for CaO (99.37%) and 30CaO@CeO₂ (97.6%). Furthermore, the concentration of the catalyst played an important role in optimizing the FAME yield in the transesterification reaction. From Figure 8, it can be seen that the biodiesel yield increased with the increase in CaO concentration, which increased from 30% w/w to 50% w/w on CeO₂ as a solid base catalyst, and the biodiesel yield also slightly decreased with further increases in CaO catalyst concentration. The optimal catalyst was determined to be 30CaO@CeO₂ with a biodiesel yield of 97.6%. The excess catalyst slightly reduced the biodiesel yield due to soap formation in the presence of a large amount of catalyst [43]. Moreover, an excess amount of catalyst results in an increase in the viscosity of the reactants, thus leading to a reduction in biodiesel production, as reported by Yang et al. [44].

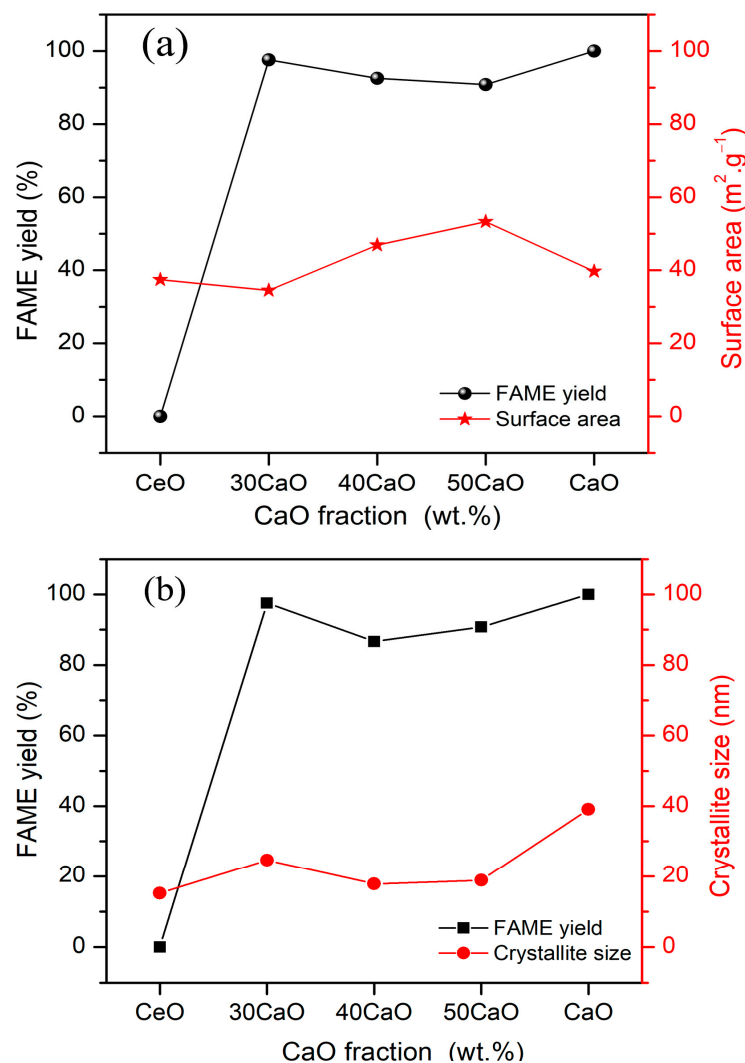


Figure 8. Correlation between (a) surface area and biodiesel yield and (b) crystallite size and biodiesel yield of CaO@CeO₂ catalysts.

Figure 9 shows the effect of reaction time on the biodiesel production for CaO and 30CaO@CeO₂. For the CaO catalysts, the results revealed that increasing the reaction time increased the FAME yield for the first 2 h and slowly decreased toward reaching equilibrium. Meanwhile, the highest FAME yield from 30CaO@CeO₂ was recorded in 30 min of reaction time, which was the maximum conversion of palm oil to biodiesel production. It was confirmed that the high FAME yields of the CaO catalysts were achieved by prolonging the reaction time when compared with the 30CaO@CeO₂ catalysts.

CaO on a CeO₂ substrate was found to produce more biodiesel than CaO without a substrate [45] due to calcium oxide diffusion into the pores and surrounding substrate surface, resulting in an increased number of active sites [46], and led to high catalytic performance via a shorter reaction time in transesterification during biodiesel production. In addition, cerium oxide was used as a support for various oxides, improving the catalytic performance through a CaO-CeO₂ interaction and a better diffusion of active metal components. As a result, 30CaO@CeO₂ was selected as the most efficient catalyst, with a catalytic activity of 97.6%. The high catalytic activity of CaO@CeO₂ catalyst was related to its amount of CaO (by wt.%) and crystallite size.

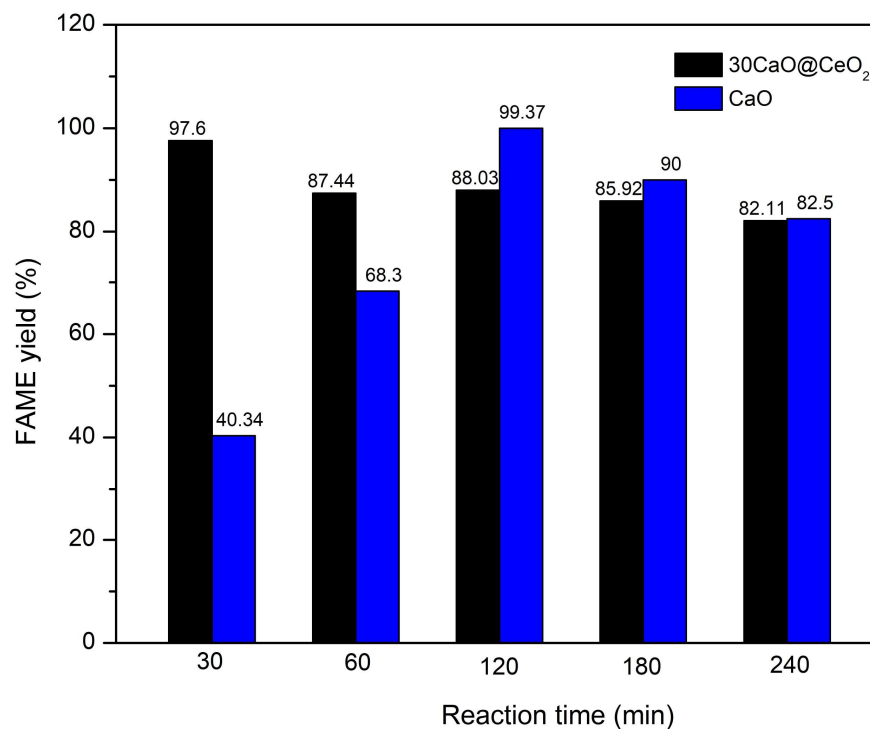


Figure 9. Effect of reaction time on biodiesel production for CaO and 30CaO@CeO₂.

2.3. Reusability

One of the most important factors for a heterogeneous catalyst's commercialization is reusability. Reusability refers to the ability of a catalyst to be used multiple times without significant loss of activity or selectivity [47]. This is crucial for reducing costs and increasing the overall efficiency of industrial processes. As bulk CaO exhibits potential as a solid base catalyst in the production of biodiesel, its limited reusability continues to be a significant drawback in this context. An evaluation of the 30CaO@CeO₂, 40CaO@CeO₂, and 50CaO@CeO₂ mixed-oxide catalysts' reusability was carried out to determine their potential utilization within the biodiesel industry. The effect of the mixed-oxide catalysts' reusability on biodiesel yield in the transesterification reaction is shown in Figure 10. After filtering, the catalysts were reused without undergoing any further post-treatment. For the CaO catalysts, there was a decreasing trend in biodiesel yield with each new reaction, with the yield decreasing from 99.37% for the first reaction to 82.62% over three cycles. The experimental data provide support that the catalyst, in its initial state, can be effectively reactivated and reused for commercial biodiesel production.

The yield decreases steadily from the beginning of the reuse. According to previous research, Wong et al. [11] have reported that the catalytic activity of CaO generally decreases rapidly for seven cycles. This loss of catalyst activity may be attributed to the dissolution of bulk CaO in the reaction media during the transesterification reaction [38], which is consistent with this research. On the other hand, the 30CaO@CeO₂ mixed-oxide catalyst output declined more gradually in biodiesel production, and it still maintained a level of over 90% after three cycles. It can be seen that the 30CaO@CeO₂ mixed-oxide catalyst had a better performance than both the 40CaO@CeO₂ catalyst and the 50CaO@CeO₂ catalyst. In general, the deactivation of CaO-based catalysts may be attributed to two main factors that affect the process: (a) CaO leaching into the reaction media and (b) the adsorption of fatty acid, glycerol, or glycerides onto the active sites of catalysts [48,49].

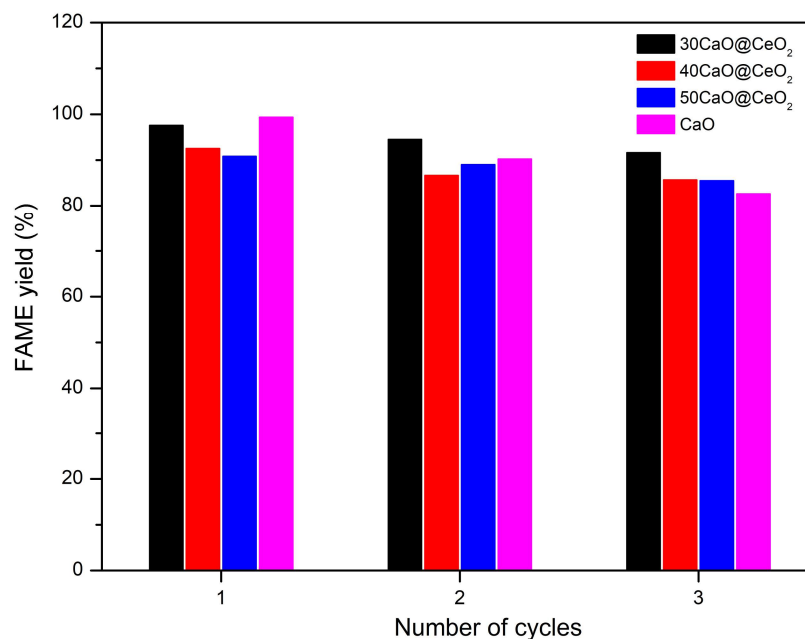


Figure 10. Effect of catalyst reusability on biodiesel yield.

3. Materials and Methods

3.1. Materials

Ce in ethylenediaminetetraacetic acid solution (Ce in EDTA solution) was obtained from the Thai monazite using the ion exchange chromatography technique. CeO₂ was obtained by the precipitation method using 3% *w/v* oxalic solution in Ce EDTA solution and calcined at 600 °C for 3 h. Calcium oxide (CaO) was obtained from Kemaus (Cherrybrook, NSW, Australia) Co., Ltd. The palm oil was purchased from a commercial company (Palm Oil Morakot Brand, Bangkok, Thailand).

3.2. Catalyst Preparation and Characterization

The catalysts containing 0, 30, 40, and 50 wt.% CaO were prepared using the wet impregnation method and designated *x*CaO@CeO₂, where *x* = 30, 40, and 50 wt.% CaO. An appropriate amount of calcium oxide was dissolved in 100 mL of distilled water. Then, 5 g of CeO₂ was gradually supplemented into the solution and continuously stirred to form a homogeneous solution. To remove excess water, the mixture was gently heated before being dried in an oven at 100 °C for 12 h. After drying, the sample was calcined at 600 °C for 3 h to obtain *x*CaO@CeO₂ catalysts. The catalyst preparation process is shown in Figure 11. Major oxides and chemical compositions were identified using wavelength dispersive X-ray fluorescence (WD-XRF, Bruker S8 Tiger, Karlsruhe, Germany). The crystal structures and crystallite sizes of catalysts were identified using an X-ray diffraction spectrometer (XRD, Bruker-AXS D8 ADVANCE model, Karlsruhe, Germany) equipped with a Cu K α radiation source at 40 kV and 40 mA. The average crystallite sizes of the catalysts were calculated by the Debye–Scherrer equation [50] as shown in Equation (1).

$$D = \frac{k\lambda}{\beta \cos \theta} \quad (1)$$

where *D* is the average crystallite size, λ is the wavelength of the X-ray source (1.5418 Å), β is the reflection width (2θ), θ is the Bragg angle, and *K* is the shape constant (0.89).

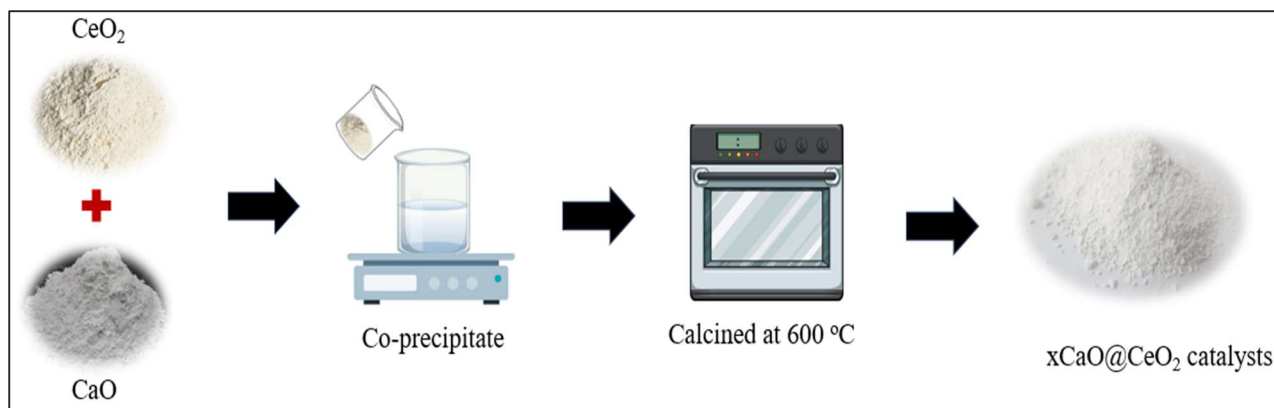


Figure 11. Schematic of catalyst preparation process.

The Fourier transform infrared spectroscopy (FTIR) was performed using the KBr pellet technique on a Perkin Elmer Spectrum Spotlight 300 in the region from 4000 to 400 cm^{-1} with a resolution of 4 cm^{-1} . Thermogravimetric analysis (TGA) was carried out using a Mettler Toledo TGA/DSC2 (Mettler Toledo, Nänikon, Switzerland) in the temperature range of 25–800 $^{\circ}\text{C}$ at a continuous heating rate of 10 $^{\circ}\text{C}/\text{min}$. The isotherms of nitrogen adsorption–desorption was evaluated using a Micromeritics 3Flex physisorption analyzer at -196°C . Prior to the adsorption studies, samples were degassed at 300 $^{\circ}\text{C}$ for 2 h under vacuum to eliminate adsorbed species from the catalyst surface. The Brunauer–Emmett–Teller (BET) and Barrett–Joyner–Halenda (BJH) methods were used to determine the surface areas and pore size distributions of the catalysts, respectively.

3.3. Transesterification Reaction

The transesterification reaction between palm oil and methanol was performed using a three-necked glass reactor including a reflux condenser and a magnetic bar stirrer. The process of biodiesel production was carried out using 100 g of palm oil and 5 wt.% modified xCaO@CeO_2 , CaO, and CeO_2 catalyst was added using the oil-to-methanol molar ratio of 1:9 and a reaction temperature of 65 $^{\circ}\text{C}$ for 30–240 min. After the transesterification reaction was completed, the catalysts were then separated by centrifuging at 6000 rpm for 30 min. For phase separation, the biodiesel products were placed in a separatory funnel. Biodiesel floated on the surface layer, while glycerol settled at the bottom. Then, the biodiesel was refined using distillation to eliminate excess methanol. Gas chromatography–mass spectrometry (Shimadzu GC-MS QP 2020, Tokyo, Japan) with a capillary column (Rxi-5Sil MS 30 m, 0.25 mm ID, 0.25 μm) was used to measure the fatty acid methyl esters (FAMES) produced after the transesterification reaction in accordance with EN 14103 standard procedure [51,52]. The schematic diagram of biodiesel production process is demonstrated in Figure 12.

Methyl heptadecanoate was used as an internal reference for this measurement according to the EN 14103 standard procedure [51,52]. The biodiesel yield was calculated using Equation (2):

$$C = \frac{(\sum A) - A_{\text{Ei}}}{A_{\text{Ei}}} \times \frac{C_{\text{Ei}} \times V_{\text{Ei}}}{m} \times 100\% \quad (2)$$

where C is fatty acid methyl ester (FAME) content, $\sum A$ is the total peak area from FAME C14 to C24, A_{Ei} is the peak area of methyl heptadecanoate, C_{Ei} is the concentration in mg/mL of the methyl heptadecanoate solution, V_{Ei} is the volume in mL of the methyl heptadecanoate solution, and m is the mass of the sample (mg). To determine the catalyst's reusability and regeneration, the catalysts were centrifuged from the post-reaction mixture, washed several times with methanol, and dried at 100 $^{\circ}\text{C}$ for 24 h. The FAME yield was measured using the procedures described above.

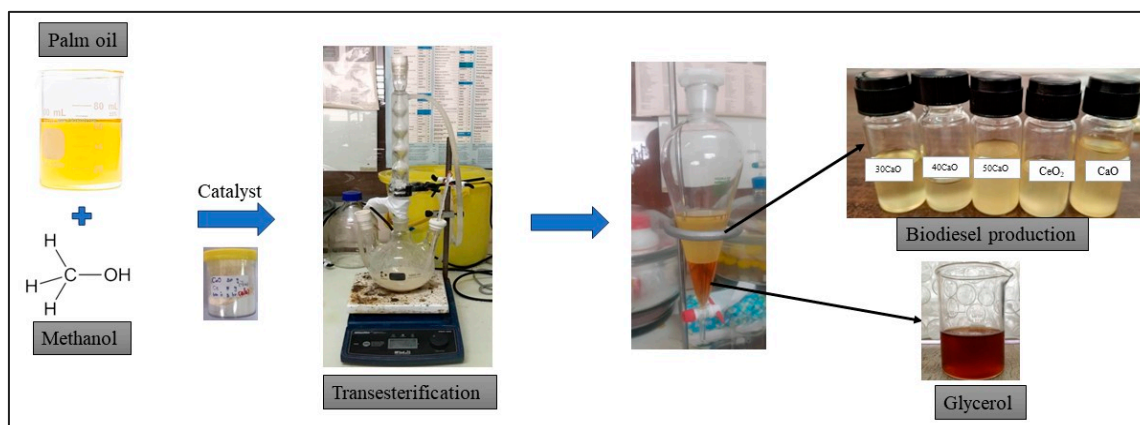


Figure 12. Schematic diagram of biodiesel production from palm oil with modified $x\text{CaO}@CeO_2$ catalysts.

4. Conclusions

The $\text{CaO}@CeO_2$ solid base catalysts prepared via the wet impregnation method were effectively applied in the biodiesel transesterification process. Cerium oxide as a support material can improve heterogeneous catalytic stability and activity due to the defects induced by the replacement of Ca ions with Ce ions on the surface of catalysts. The optimum catalyst was $30\text{CaO}@CeO_2$ considering the catalytic activity and surface properties, resulting in the highest FAME yield of 97.6%. In addition, the catalyst could be reused up to three times with good activity, achieving a FAME yield of over 90%. Additionally, compared to CaO without doping CeO_2 , the advantage of utilizing $30\text{CaO}@CeO_2$ in this result can demonstrate a short reaction time to receive the greatest yield. The excellent performance of this catalyst in transesterification reactions was possibly due to the strong synergic interaction between CeO_2 and CaO. This interaction was attributed to the structure of these samples, with Ce embedded in calcium oxide. However, the high surface area of the catalysts was not a direct factor in the catalytic activity that resulted in the transesterification reaction of $\text{CaO}@CeO_2$ to biodiesel. CeO_2 can decrease the amount of calcium that leaches into the product phase, stabilize the active phases, and increase the catalyst's stability through the reactions. The test results reveal that the $\text{CaO}@CeO_2$ solid base catalysts may have good potential for large-scale biofuel production in industries, as well as reusability. They also suggest that a $\text{CaO}@CeO_2$ material has potential as a catalyst for the environmentally friendly biodiesel production process.

Author Contributions: Conceptualization, W.K.; methodology, J.M. and K.K.; validation, W.K. and S.N.; formal analysis, D.R. and W.K.; investigation, K.N., J.M. and S.I.; data curation, J.M., K.K. and K.N.; writing—original draft preparation, W.K. and S.I.; writing—review and editing, all authors; supervision, D.R., S.N. and W.K.; project administration, W.K.; funding acquisition, W.K. All authors have read and agreed to the published version of the manuscript.

Funding: This research was funded by the Thailand Science Research and Innovation (Fundamental Fund, grant number 4697347).

Data Availability Statement: The data presented in this study are available on request from the corresponding author.

Acknowledgments: The authors would like to thank the Thailand Institute of Nuclear Technology (Public Organization) for the useful suggestions and provide the instrument.

Conflicts of Interest: The authors declare no conflicts of interest.

References

1. Aghahosseini, A.; Breyer, C. Assessment of geological resource potential for compressed air energy storage in global electricity supply. *Energy Convers. Manag.* **2018**, *169*, 161–173. [[CrossRef](#)]
2. Strielkowski, W.; Civín, L.; Tarkhanova, E.; Tvaronavičienė, M.; Petrenko, Y. Renewable energy in the sustainable development of electrical power sector: A review. *Energies* **2021**, *14*, 8240. [[CrossRef](#)]
3. Qi, D.H.; Chen, H.; Matthews, R.D.; Bian, Y.Z. Combustion and emission characteristics of ethanol–biodiesel–water micro-emulsions used in a direct injection compression ignition engine. *Fuel* **2010**, *89*, 958–964. [[CrossRef](#)]
4. Nasreen, S.; Nafees, M.; Qureshi, L.A.; Asad, M.S.; Sadiq, A.; Ali, S.D. Review of catalytic transesterification methods for biodiesel production. *Biofuels State Dev.* **2018**, *6*, 93–119.
5. López, D.E.; Goodwin, J.G., Jr.; Bruce, D.A.; Lotero, E. Transesterification of triacetin with methanol on solid acid and base catalysts. *Appl. Catal. A Gen.* **2005**, *295*, 97–105. [[CrossRef](#)]
6. Sronsri, C.; Sittipol, W.; Kongpop, U. Optimization of biodiesel production using magnesium pyrophosphate. *Chem. Eng. Sci.* **2020**, *226*, 115884. [[CrossRef](#)]
7. Vujicic, D.; Comic, D.; Zarubica, A.; Micic, R.; Boskovic, G. Kinetics of biodiesel synthesis from sunflower oil over CaO heterogeneous catalyst. *Fuel* **2010**, *89*, 2054–2061. [[CrossRef](#)]
8. Hattori, H.; Shima, M.; Kabashima, H. Alcoholysis of ester and epoxide catalyzed by solid base. *Stud. Surf. Sci. Catal.* **2000**, *130*, 3507–3512.
9. Taufiq-Yap, Y.H.; Lee, H.V.; Yunus, R.; Juan, J.C. Transesterification of non-edible *Jatropha curcas* oil to biodiesel using binary Ca–Mg mixed oxide catalyst: Effect of stoichiometric composition. *Chem. Eng. J.* **2011**, *178*, 342–347. [[CrossRef](#)]
10. Wu, T.; Guo, R.T.; Li, C.F.; Pan, W.G. Recent progress of CeO₂-based catalysts with special morphologies applied in air pollutants abatement: A review. *J. Environ. Chem. Eng.* **2023**, *11*, 109136. [[CrossRef](#)]
11. Wong, Y.C.; Tan, Y.P.; Taufiq-Yap, Y.H.; Ramli, I.; Tee, H.S. Biodiesel production via transesterification of palm oil by using CaO–CeO₂ mixed oxide catalysts. *Fuel* **2015**, *162*, 288–293. [[CrossRef](#)]
12. Kawashima, A.; Matsubara, K.; Honda, K. Development of heterogeneous catalysts for biodiesel production. *Bioresour. Technol.* **2008**, *99*, 3439–3443. [[CrossRef](#)] [[PubMed](#)]
13. Reyero, I.; Moral, A.; Bimbela, F.; Radosevic, J.; Sanz, O.; Montes, M.; Gandía, L.M. Metallic monolithic catalysts based on calcium and cerium for the production of biodiesel. *Fuel* **2016**, *182*, 668–676. [[CrossRef](#)]
14. Thitsartarn, W.; Kawi, S. An active and stable CaO–CeO₂ catalyst for transesterification of oil to biodiesel. *Green Chem.* **2011**, *13*, 3423–3430. [[CrossRef](#)]
15. Zhang, N.; Xue, H.; Hu, R. The activity and stability of CeO₂@CaO catalysts for the production of biodiesel. *RSC Adv.* **2018**, *8*, 32922–32929. [[CrossRef](#)] [[PubMed](#)]
16. Qin, F.; Nohair, B.; Shen, W.; Xu, H.; Kaliaguine, S. Promotional effects of CeO₂ on stability and activity of CaO for the glycerolysis of triglycerides. *Catal. Lett.* **2016**, *146*, 1273–1282. [[CrossRef](#)]
17. Montini, T.; Melchionna, M.; Monai, M.; Fornasiero, P. Fundamentals and catalytic applications of CeO₂-based materials. *Chem. Rev.* **2016**, *116*, 5987–6041. [[CrossRef](#)] [[PubMed](#)]
18. Yu, X.; Wen, Z.; Li, H.; Tu, S.T.; Yan, J. Transesterification of *Pistacia chinensis* oil for biodiesel catalyzed by CaO–CeO₂ mixed oxides. *Fuel* **2011**, *90*, 1868–1874. [[CrossRef](#)]
19. Mehdipour-Ataei, S.; Aram, E. Mesoporous Carbon-Based Materials: A Review of Synthesis, Modification, and Applications. *Catalysts* **2022**, *13*, 2. [[CrossRef](#)]
20. Bayne, L.; Ulijn, R.V.; Halling, P.J. Effect of pore size on the performance of immobilised enzymes. *Chem. Soc. Rev.* **2013**, *42*, 9000–9010. [[CrossRef](#)]
21. Maroa, S.; Inambao, F. A review of sustainable biodiesel production using biomass derived heterogeneous catalysts. *Eng. Life Sci.* **2021**, *21*, 790–824. [[CrossRef](#)] [[PubMed](#)]
22. Laskar, I.B.; Deshmukhya, T.; Biswas, A.; Paul, B.; Changmai, B.; Gupta, R.; Chatterjee, S.; Rokhum, S.L. Utilization of biowaste-derived catalysts for biodiesel production: Process optimization using response surface methodology and particle swarm optimization method. *Energy Adv.* **2022**, *1*, 287–302. [[CrossRef](#)]
23. Kingkam, W.; Nilgumhang, K.; Nuchdang, S.; Duangdee, B.; Puripunyanich, V.; Rattanaphra, D. Study the Stable Diatomite-supported Catalyst for Biodiesel Production. *Chiang Mai J. Sci.* **2022**, *49*, 1332–1343. [[CrossRef](#)]
24. Zhao, L.; Qin, H.; Wu, R.A.; Zou, H. Recent advances of mesoporous materials in sample preparation. *J. Chromatogr. A.* **2012**, *1228*, 193–204. [[CrossRef](#)] [[PubMed](#)]
25. Mach, T.P.; Ding, Y.; Binder, J.R. Impact of Particle and Crystallite Size of Ba_{0.6}Sr_{0.4}TiO₃ on the Dielectric Properties of BST/P (VDF-TrFE) Composites in Fully Printed Varactors. *Polymers* **2022**, *14*, 5027. [[CrossRef](#)] [[PubMed](#)]
26. Nandiyanto, A.B.D.; Zaen, R.; Oktiani, R. Correlation between crystallite size and photocatalytic performance of micrometer-sized monoclinic WO₃ particles. *Arab. J. Chem.* **2020**, *13*, 1283–1296. [[CrossRef](#)]
27. Thunyaratchatanon, C.; Jitjamnong, J.; Luengnaruemitchai, A.; Numwong, N.; Chollacoop, N.; Yoshimura, Y. Influence of Mg modifier on cis-trans selectivity in partial hydrogenation of biodiesel using different metal types. *Appl. Catal. A Gen.* **2016**, *520*, 170–177. [[CrossRef](#)]
28. Anjalini, M.; Kanagathara, N.; Suganthi, A.R.B. A Brief Review on Aniline and Its Derivatives. *Mater. Today Proc.* **2020**, *33*, 4751–4755. [[CrossRef](#)]

29. Fatimah, I.; Fadillah, G.; Sagadevan, S.; Oh, W.C.; Ameta, K.L. Mesoporous Silica-Based Catalysts for Biodiesel Production: A Review. *Chem. Eng.* **2023**, *7*, 56. [[CrossRef](#)]
30. Safat, S.; Buazar, F.; Albukhaty, S.; Matroodi, S. Enhanced sunlight photocatalytic activity and biosafety of marine-driven synthesized cerium oxide nanoparticles. *Sci. Rep.* **2021**, *11*, 14734. [[CrossRef](#)]
31. Mirghiasi, Z.; Bakhtiari, F.; Darezereshki, E.; Esmaeilzadeh, E. Preparation and characterization of CaO nanoparticles from Ca(OH)₂ by direct thermal decomposition method. *J. Ind. Eng. Chem.* **2014**, *20*, 113–117. [[CrossRef](#)]
32. Mazher, M.; Ishtiaq, M.; Hamid, B.; Haq, S.M.; Mazhar, A.; Bashir, F.; Mazhar, M.; Mahmoud, E.A.; Casini, R.; Alataway, A.; et al. Biosynthesis and characterization of Calcium Oxide nanoparticles from Citrullus colocynthis Fruit extracts; their biocompatibility and bioactivities. *Materials* **2023**, *16*, 2768. [[CrossRef](#)] [[PubMed](#)]
33. Maneerung, T.; Kawi, S.; Dai, Y.; Wang, C.H. Sustainable biodiesel production via transesterification of waste cooking oil by using CaO catalysts prepared from chicken manure. *Energy Conv. Manag.* **2016**, *123*, 487–497. [[CrossRef](#)]
34. Manurung, R.; Parinduri, S.Z.D.M.; Hasibuan, R.; Tarigan, B.H.; Siregar, A.G.A. Synthesis of nano-CaO catalyst with SiO₂ matrix based on palm shell ash as catalyst support for one cycle developed in the palm biodiesel process. *Case Stud. Chem. Environ. Eng.* **2023**, *7*, 100345. [[CrossRef](#)]
35. Loy, C.W.; Amin Matori, K.; Lim, W.F.; Schmid, S.; Zainuddin, N.; Abdul Wahab, Z.; Nadakkavil Alassan, Z.; Mohd Zaid, M.H. Effects of calcination on the crystallography and nonbiogenic aragonite formation of ark clam shell under ambient condition. *Adv. Mater. Sci. Eng.* **2016**, *2016*, 2914368. [[CrossRef](#)]
36. Habib, S.; Fayyad, E.; Nawaz, M.; Khan, A.; Shakoor, R.A.; Kahraman, R.; Abdullah, A. Cerium dioxide nanoparticles as smart carriers for self-healing coatings. *Nanomaterials* **2020**, *10*, 791. [[CrossRef](#)] [[PubMed](#)]
37. Giammaria, G.; Lefferts, L. Catalytic effect of water on calcium carbonate decomposition. *J. CO₂ Util.* **2019**, *33*, 341–356. [[CrossRef](#)]
38. Basumatary, S.F.; Brahma, S.; Hoque, M.; Das, B.K.; Selvaraj, M.; Brahma, S.; Basumatary, S. Advances in CaO-based catalysts for sustainable biodiesel synthesis. *Green Energy Resour.* **2023**, *1*, 100032. [[CrossRef](#)]
39. Zheng, H.; He, Y.; Zhu, Y.; Liu, L.; Cui, X. Novel procedure of CO₂ capture of the CaO sorbent activator on the reaction of one-part alkali-activated slag. *RSC. Adv.* **2021**, *11*, 12476–12483. [[CrossRef](#)]
40. Teo, S.H.; Rashid, U.; Taufiq-Yap, Y.H. Heterogeneous catalysis of transesterification of jatropha curcas oil over calcium–cerium bimetallic oxide catalyst. *RSC. Adv.* **2014**, *4*, 48836–48847. [[CrossRef](#)]
41. Pranata, D.E.; Syarif, A.; Yerizam, M. Characterization of Fly Ash Catalyst Using XRD Method for Biofuel Production from Used Cooking Oil. *Indones. J. Fundam. Appl. Chem.* **2021**, *6*, 90–95. [[CrossRef](#)]
42. Poonanan, A.; Prukpaiboon, A.; Dim, P.E.; Termtanun, M. Using shrimp shells as based catalysts for FAME production from palm oil feedstock. *J. Met. Mater. Miner.* **2021**, *31*, 78–83. [[CrossRef](#)]
43. Ismail, S.; Ahmed, A.S.; Anr, R.; Hamdan, S. Biodiesel production from castor oil by using calcium oxide derived from mud clam shell. *J. Renew. Energy* **2016**, *2016*, 5274917. [[CrossRef](#)]
44. Yang, F.X.; Su, Y.Q.; Li, X.H.; Zhang, Q.; Sun, R.C. Preparation of biodiesel from *Idesia polycarpa* var. *vestita* fruit oil. *Ind. Crops. Prod.* **2009**, *29*, 622–628. [[CrossRef](#)]
45. Wu, H.; Zhang, J.; Wei, Q.; Zheng, J.; Zhang, J. Transesterification of soybean oil to biodiesel using zeolite supported CaO as strong base catalyst. *Fuel Process Technol.* **2013**, *109*, 13–18. [[CrossRef](#)]
46. Sohn, J.R.; Park, E.H. Acidic properties of CaO binary oxide catalyst and Activity for acid catalysis. *Korean J. Chem. Eng.* **1997**, *14*, 192–197. [[CrossRef](#)]
47. Mandari, V.; Devarai, S.K. Biodiesel production using homogeneous, heterogeneous, and enzyme catalysts via transesterification and esterification reactions: A critical review. *Bioenergy Res.* **2022**, *15*, 935–961. [[CrossRef](#)] [[PubMed](#)]
48. Kouzu, M.; Hidaka, J.S. Transesterification of vegetable oil into biodiesel catalyzed by CaO: A review. *Fuel* **2012**, *93*, 1–12. [[CrossRef](#)]
49. Oueda, N.; Bonzi-Coulibaly, Y.L.; Ouédraogo, I.W. Deactivation processes, regeneration conditions and reusability performance of CaO or MgO based catalysts used for biodiesel production—A review. *Mater. Sci. Appl.* **2016**, *8*, 94–122. [[CrossRef](#)]
50. Holzwarth, U.; Gibson, N. The Scherrer equation versus the ‘Debye-Scherrer equation’. *Nat. Nanotechnol.* **2011**, *6*, 534. [[CrossRef](#)]
51. Tercini, A.C.B.; Pinesi, M.; Calera, G.C.; Sequinel, R.; Hatanaka, R.R.; de Oliveira, J.E.; Flumignan, D.L. Ultrafast gas chromatographic method for quantitative determination of total FAMES in biodiesel: An analysis of 90 s. *Fuel* **2018**, *222*, 792–799. [[CrossRef](#)]
52. Barbosa, S.L.; Rocha, A.C.P.; Nelson, D.L.; de Freitas, M.S.; Mestre, A.A.F.; Klein, S.L.; Clososki, G.C.; Caires, F.J.; Flumignan, D.L.; Dos Santos, L.K.; et al. Catalytic transformation of triglycerides to biodiesel with SiO₂-SO₃H and quaternary ammonium salts in toluene or DMSO. *Molecules* **2022**, *27*, 953. [[CrossRef](#)] [[PubMed](#)]

Disclaimer/Publisher’s Note: The statements, opinions and data contained in all publications are solely those of the individual author(s) and contributor(s) and not of MDPI and/or the editor(s). MDPI and/or the editor(s) disclaim responsibility for any injury to people or property resulting from any ideas, methods, instructions or products referred to in the content.